J Mol Model (2013) 19:1565–1572
DOI 10.1007/s00894-012-1718-3

ORIGINAL PAPER

Mechanistic investigations of $Al(OH)_3$ oligomerization mechanisms

Xueli Cheng · Wenchao Ding · Yongjun Liu · Dairong Chen

Received: 21 August 2012 / Accepted: 29 November 2012 / Published online: 28 December 2012

Abstract Aluminum aerogels have extremely low thermal conductivities, and are ideal candidates for use in thermal superinsulators, adsorbents, sensors, catalyst carriers, and inorganic fillers. In the present work, the oligomerization mechanisms of $Al(OH)_3$ were investigated systematically with the Gaussian 03 package at the B3LYP/6-311++G(d,p) level in combination with CPCM single-point energy calculations. The results of our theoretical model showed that: (1) the Al atoms are tetracoordinate and pentacoordinate; (2) in alkaline solution, $Al(OH)_3$ tends to condense into more soluble polyhydroxy compounds; (3) the neutral dimerization of $Al(OH)_3$ and the transfer of the hydrogen on the bridging hydroxyl are energetically favorable, but the most stable geometry is a four-membered Al–O ring structure linked by two bridging hydroxyls; (4) $Al(OH)_3$ is inclined to form tetracoordinate oligomers, which develop into three-dimensional structures connected by four-membered Al–O rings.

Keywords Oligomerization · $Al(OH)_3$ · B3LYP · Aluminum aerogels

Introduction

Aerogels are a class of low-density and nanoporous materials that are obtained through the aggregation of nanoparticles or polymer molecules and consist of a porous framework filled with gas molecules [1–3]. As a result, aerogels—which were first reported by Kistler in 1931 [4]—are also known as frozen smoke. Currently, aerogels that are synthesized via the hydrolysis, oligomerization, gelation, aging, desiccation, and densification of various alkoxide precursors possess desirable physical properties such as low thermal conductivity, high acoustic impedance, large specific surface area, and a low relative dielectric constant, and thus are ideal candidates for use in thermal superinsulators, adsorbents, sensors, catalyst carriers, and inorganic fillers [5–9]. Among the various metal aquasols available, aluminum aerogels have extremely low thermal conductivities, and have the potential for broad application in launch vehicles and manned spacecraft to protect the instruments and humans inside from damage/injury due to high temperatures [10].

Experimental and theoretical investigations concerning aerogels have mostly focused on silicon compounds, which are noncrystalline aerogels, in recent years [11]. Al_2O_3 aerogels are crystalline aerogels that can be synthesized from aluminum alkoxide precursors [12]. Although $Al(OH)_3$ and Al_2O_3 have been widely applied to prepare a variety of materials with unique properties [13–15], and nanostructures of $Al(OH)_3$ and Al_2O_3 have already attracted much attention [16], there has been a lack of investigation of the evolution and formation mechanisms of Al_2O_3 aerogels [17]. $Al(OH)_3$ can be acquired by hydrolyzing aluminum alkoxides; indeed, it is very easy to hydrolyze them to $Al(OH)_3$ [10, 18]. It is therefore important from a practical perspective to probe the condensation mechanisms of $Al(OH)_3$ as a reaction template for the microstructural evolution of Al_2O_3 aquasols. Aluminum alkoxide precursors are electron-deficient compounds that are inclined to coordinate with water and alcohols. Therefore, if aluminum alkoxides are employed as precursors to assemble aerogels, the associated hydrolysis and oligomerization mechanisms will be unique. Moreover, identifying the Al coordination structure is an intricate problem [19] that has attracted much attention (e.g., the pioneering work of Laasonen's group [20–23]). Studies

Electronic supplementary material The online version of this article (doi:10.1007/s00894-012-1718-3) contains supplementary material, which is available to authorized users.

W. Ding · Y. Liu (✉) · D. Chen
School of Chemistry and Chemical Engineering, Shandong University, Jinan 250100, China
e-mail: yongjunliu_1@sdu.edu.cn

X. Cheng
School of Chemistry and Chemical Engineering, Taishan University, Tai'an 271021, China

investigating the coordination modes and forms of Al^{3+} are therefore very valuable, as are those that focus on $Al(OH)_3$ oligomerization mechanisms in the sol–gel processes of aluminum alkoxides. Therefore, in the present work, we employed density functional theory (DFT) to investigate the coordination modes and condensation mechanisms of $Al(OH)_3$.

Computational details

In this work, all species were fully optimized and frequency calculations was performed at the B3LYP/6-311++G(d,p) basis set level with the Gaussian 03 program package [24] to obtain the zero-point energies (ZPE) and to identify whether the stationary point is a local minimum or a transition state. Density functional theory has already been successfully applied to molecular systems containing Al atoms, and the results yielded by DFT have been extensively compared with those obtained using various other methods [25–29]. B3LYP has also proven to be a reliable method of optimizing molecular structures and elucidating reaction mechanisms [10, 16, 30–36]. Furthermore, the displacement vectors of the imaginary vibrational modes have been used to identify real transition states and their connections [37], and some key transition states have also been checked by intrinsic reaction coordinate (IRC) calculations to confirm the connections between the corresponding intermediates [38, 39].

The liquid environment was modeled with the conductor-like screening model (CPCM) [40, 41] in order to account for the effects of bulk water, with water represented as a dielectric continuum. To reduce computational times, CPCM single-point energy (SPE) calculations were carried out with the gas-phase equilibrium geometries at the same basis set level of theory without frequency calculations, and then the single-point Gibbs free energies were scaled with the ZPE in the gas phase. The united atom Kohn–Sham (UAKS) theory was used to define the atomic radii in the SPE calculations since water has a high dielectric constant ($\varepsilon = 78.35$) [42–46]. Because diffuse functions were employed, we used the SCF=Tight keyword to request tight SCF convergence criteria in the SPE calculations in an attempt to improve the accuracy. Furthermore, to account for the effects of entropy, we employed the entropy values obtained in the gas phase to calibrate the relative free energies of the SPE calculations from 0 K to 298.15 K, and compared them with the values obtained before entropy correction.

To validate the reliability of the theoretical model, the coordination modes and forms of $Al(OH)_3$ present in neutral solution were investigated by full optimization combined with the CPCM solvation model at the M06-2X/6-311++G(d,p) level using the Gaussian 09 package, due to the good performance of the M06-2X functional when applied to main-group thermochemistry [47, 48]. Frequency calculations were also performed at the same basis set level of theory.

Results and discussion

The lowest frequencies and their vibrational mode assignments as well as the Gibbs free energies scaled with the zero-point energies in the gas phase for all species investigated in the present work are listed in Table S1 of the "Electronic supplementary material" (ESM). First of all, we confirmed the coordination modes and forms of $Al(OH)_3$ present in neutral solution, and then we ascertained its oligomerization mechanisms. In the present work, the orientations of different hydrogen-bonding arrays were utilized to facilitate the condensation process. Because aluminum alkoxides and $Al(OH)_3$ tend to form soluble compounds in alkaline solution, we focused mainly on the $Al(OH)_3$ condensation mechanisms in neutral and acidic solutions.

Coordination modes and forms of $Al(OH)_3$

Under neutral conditions, 1–6 water molecules were placed explicitly around $Al(OH)_3$. The optimized geometrical structures of these complexes and their relative free energies are depicted in Fig. 1. When one water molecule is coordinated to $Al(OH)_3$, the free energy decreases by 34.4 kJ/mol^{-1}. When two water molecules are added to $Al(OH)_3$ via coordination bonds, the energy decreases by 2.1 kJ/mol^{-1}. For $Al(OH)_3{\cdot}3H_2O$, the hexacoordinate Al species is less stable than the penta-coordinate one by 61.1 kJ/mol^{-1}, so the third water molecule does not coordinate to the central Al atom.[1] The structural parameters of hexacoordinate $Al(OH)_3{\cdot}3H_2O$ are illustrated in Fig. S1 of the ESM. For Al^{3+} in aqueous solution, Kowall et al. [49] proved the existence of a pentacoordinate intermediate $[Al(OH_2)_5{\cdot}(OH_2)]^{3+}$, and Swaddle and coworkers [19] identified a persistent pentacoordinate structure in the CPMD simulations. The addition of another water molecule to $Al(OH)_3{\cdot}2H_2O$ via two hydrogen bonds increases the free energy further by 18.6 kJ/mol^{-1}, and the further addition of water molecules decreases the energy markedly. Figure 1 illustrates that in $Al(OH)_3{\cdot}H_2O$, the length of the newly formed coordination bond is 1.988 Å, and in $Al(OH)_3{\cdot}2H_2O$, the coordination bonds lengthen to 2.092 and 2.097 Å. In the hexacoordinate $Al(OH)_3{\cdot}6H_2O$, the structure may be stabilized by three explicit water molecules [19], but

[1] Note that the hexacoordinate $Al(OH)_3{\cdot}3H_2O$ is not obtained by full optimization, but from a single-point calculation performed upon removing the three explicit water molecules in $Al(OH)_3{\cdot}6H_2O$. Full optimization will lead to the pentacoordinate species.

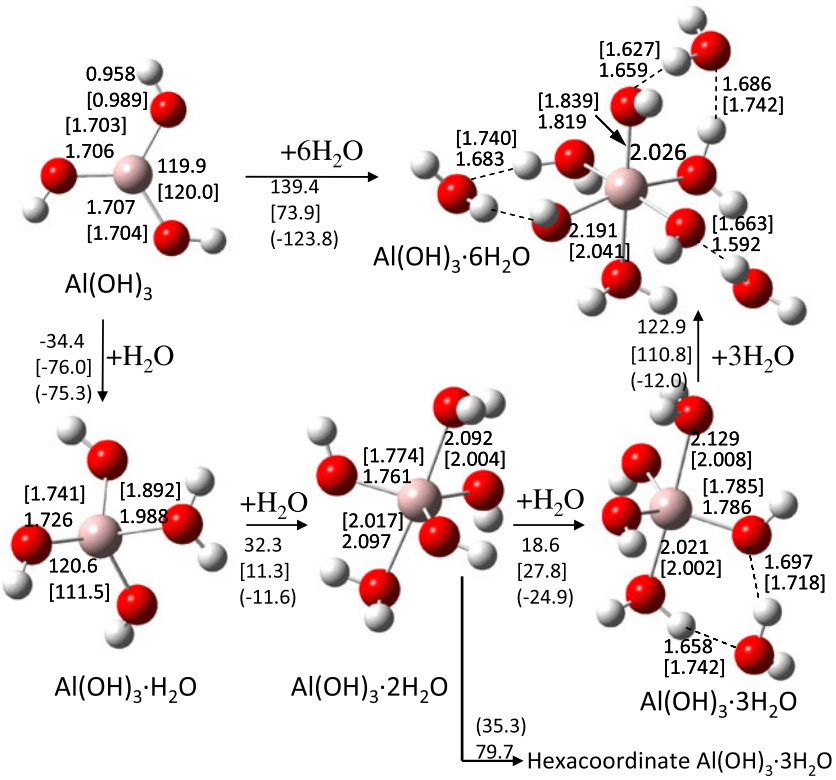

Fig. 1 Geometric parameters and free energy differences for $Al(OH)_3 \cdot nH_2O$ (n=1–6). Free energies are the CPCM SPE results corrected for entropy, but those in *parentheses* are the SPE results without any entropy correction. Structural parameters and energies in *square brackets* were obtained by full optimization with the CPCM solvation model at the M06-2X/6-311++G(d,p) level. Relative energies are in kJ/mol^{-1}, bond lengths are in Å, and bond angles are in degrees. These units are employed uniformly in all figures

the central Al atom and the three hydroxy oxygen atoms cannot maintain a planar structure. Therefore, Al atoms are tetracoordinate and pentacoordinate.

From Fig. 1, it is also apparent that full optimization with the CPCM solvation model generally maintains the framework obtained in the gas phase, but some bond lengths vary notably, especially those relating to weak interactions. The effect of entropy plays an important role when estimating the bonding free energies, and significantly influences the relative free energies. The results of full CPCM optimization at the M06-2X/6-311++G(d,p) level are consistent with the SPE results after correcting for entropy, which indicates that the B3LYP functional and our theoretical model are reliable. The energy differences between M06-2X and B3LYP may result largely from the abovementioned geometric differences. Thus, in the present work, we employed the B3LYP SPE results after entropy correction to elucidate the mechanisms of $Al(OH)_3$ oligomerization.

In alkaline solution, the complexation of OH^- and $Al(OH)_3$ to form $[Al(OH)_4]^-$ decreases the free energy significantly (by 144.6 kJ/mol^{-1}). In the present work, we assume that $[Al(OH)_4]^-$ is dehydrated to $[AlO(OH)_2]^-$ via intramolecular hydrogen transfer, as depicted in Fig. 2. However, the hydrogen-transfer barrier for $[Al(OH)_4]^-$ is as large as 207.8 kJ/mol^{-1}, and the relative free energies of the intermediates and products are all very high, suggesting that in alkaline solution, tetracoordinate Al compounds are more stable than tricoordinate ones, and the monomer does not exist in the form of $[AlO(OH)_2]^-$. The tetrahedral $[Al(OH)_4]^-$ structure prevails in alkaline solution [19, 50].

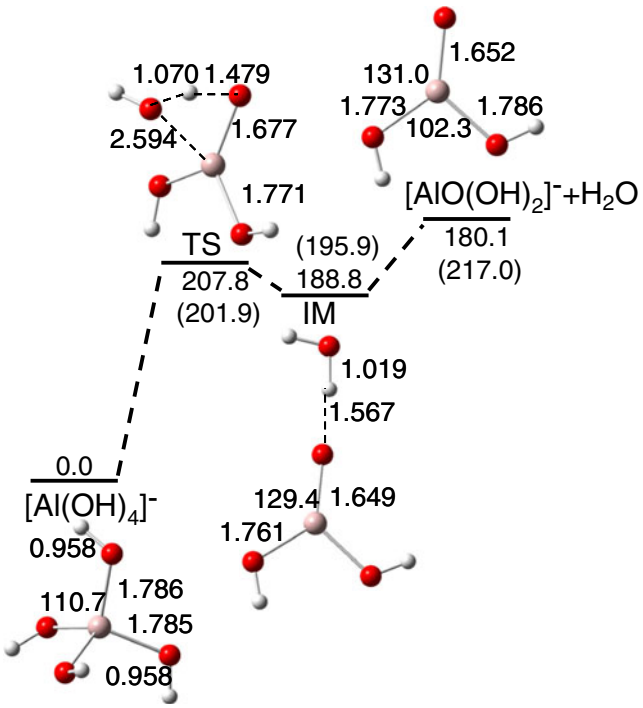

Fig. 2 Optimized structural parameters and PES profile of $[Al(OH)_4]^- \rightarrow [AlO(OH)_2]^- + H_2O$

Condensation of $Al(OH)_3$ monomer under alkaline solutions

In alkaline solution, $[Al(OH)_4]^-$ and $Al(OH)_3$ monomer initially produce the intermediate **OH1-IM1**, in which both of the two Al atoms are tetracoordinate, decreasing the free energy by 87.4 kJ/mol^{-1}, as shown in Fig. 3. The hydrogen atom on the bridging hydroxyl group can shift to the neighboring hydroxyl via **OH1-TS**, generating **OH1-IM2**. This process has a free energy barrier of 101.6 kJ/mol^{-1}, and the relative energy of **OH1-TS** is also relatively low (14.2 kJ/mol^{-1}), so it is energetically favorable. In **OH1-IM2**, the transferred hydrogen lies between the two hydroxyl groups, forming a six-membered ring. If the coordination bond of length 1.958 Å between Al and H_2O in **OH1-IM2** is broken, the free energy increases greatly, so the departure of the hydroxyl hydrogen cannot lead to dehydration.

When two $[Al(OH)_4]^-$ are linked together via two weak hydrogen bonds (with bond lengths of 2.234 and 2.235 Å), the free energy increases by 68.8 kJ/mol^{-1}. The optimized structural parameters and PES profile of two $[Al(OH)_4]^-$ anions are depicted in Fig. 4. The hydrogen atom in the hydrogen bond can be transferred via **OH2-TS** to link the two $[Al(OH)_4]^-$ by a coordination bond. The total barrier is 86.5 kJ/mol^{-1}. After the departure of the H_2O, the Al–O–Al bond angle in product **OH2-P** is nearly linear (174.8°). Figure 4 shows that the AlO_4 units tend to be separated under alkaline solutions. As a result, the monomer is inclined to form more soluble polyhydroxy compounds.

Dimerization of $Al(OH)_3$ in neutral solution

The abovementioned calculations show that, in alkaline solution, $Al(OH)_3$ exists in the form of more soluble polyhydroxy compounds in order to hinder the nucleation of aquasols, so a theoretical investigation of its condensation mechanisms in neutral solution would be valuable. Via a barrierless process, two $Al(OH)_3$ molecules produce the intermediate **d2-IM1** with a bridging hydroxyl group, reducing the free energy by −52.3 kJ/mol^{-1} (Fig. 5). Our theoretical model shows that **d2-IM1** is not cyclized via intramolecular H-transfer. However, the hydrogen atom on the bridging hydroxyl group can shift to an adjacent hydroxyl group via **d2-TS**, generating **d2-IM2**. Figure 5 shows that **d2-IM2** has the lowest free energy along the reaction coordinate, implying that the structure bridged with O atoms may be energetically favorable. With the departure of the H_2O moiety in **d2-IM2**, the free energy increases significantly.

In these dimerization mechanisms, there are unsaturated products, which can help us to understand the potential to form porous networks in aerogel fabrication. The most stable dimer, termed **d2-IM3**, is actually the structure with a four-membered Al–O ring bridged by two hydroxyl groups, which forms via a barrierless process, as shown in Fig. 5. **d2-IM3** is also produced barrierlessly, and its relative free energy is −186.2 kJ/mol^{-1} compared with $2Al(OH)_3$. **d2-IM3** is the most stable dimer in terms of free energy, and there is no dehydration channel.

Trimerization of $Al(OH)_3$ under neutral conditions

In the present work, we added $Al(OH)_3$ to the most stable dimer **d2-IM3** to investigate the condensation and stability of trimers. Three trimers were considered: **d3-IM1**, **d3-IM1**, and **d2-IM3**, as shown in Fig. 6. $Al(OH)_3$ is connected with **d2-IM3** via two hydrogen bonds to generate the trimer **d3-**

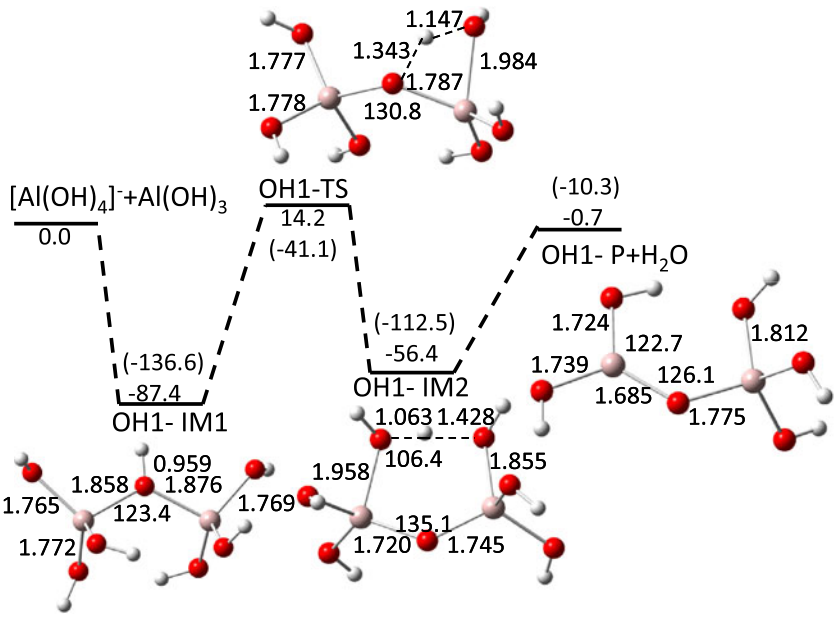

Fig. 3 Optimized structural parameters and PES profile of $[Al(OH)_4]^-+Al(OH)_3$ in alkaline solution

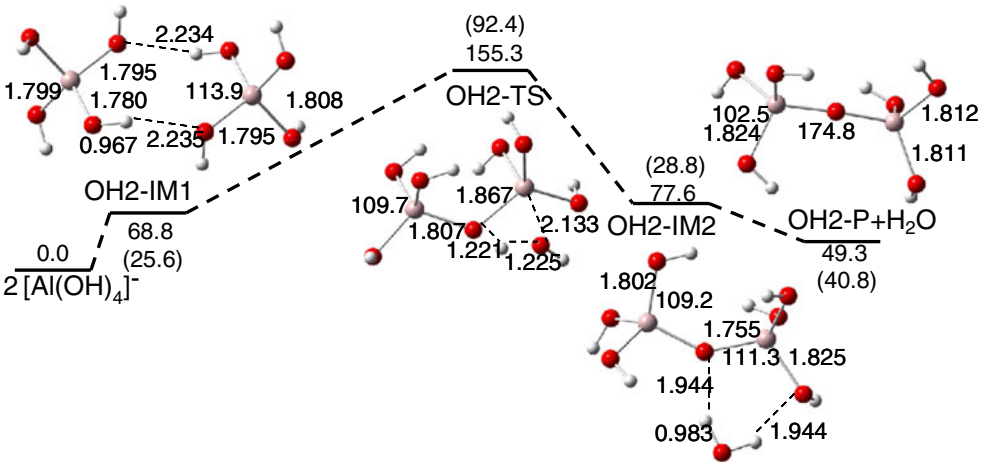

Fig. 4 Optimized structural parameters and PES profile of $2[Al(OH)_4]^-$ in alkali solution

IM1, and the S_N2 dehydration and condensation mechanism of **d3-IM1** was investigated. **d3-IM2** is the most stable trimer, and it was employed to probe the S_N1 dehydration mechanism. Isomer **d3-IM3** was used to explore whether **d2-IM3** and $Al(OH)_3$ can condense into three-dimensional cage-like/reticular structures. The formation of these three intermediates changes the free energies by 43.2, −114.8 and −66.4 kJ/mol^{-1}, respectively.

The optimized geometrical parameters and PES profile of the S_N2 condensation mechanism of **d3-IM1** are also depicted in Fig. 6. $Al(OH)_3$ links to the most stable dimer through a six-membered ring with two hydrogen bonds, forming **d3-IM1**. Then, via **d3-TS1**, and with a barrier of only 45.8 kJ/mol^{-1}, a hydrogen atom diverts from $Al(OH)_3$ to the dimer, and $Al(OH)_3$ simultaneously coordinates to the dimer to produce **d3-IM4**, as shown in Fig. 6. In **d3-IM4**, the coordination bond distance to the H_2O is 1.990 Å. The relative free energy of **d3-P1**+H_2O is −6.7 kJ/mol^{-1}, so this channel may be favored.

There is a pentacoordinate aluminum atom in **d3-IM2**, and the neighboring bridging hydroxyl hydrogen can shift to the hydroxyl group on this aluminum atom via **d3-TS2**, generating **d3-IM5**, as illustrated in Fig. 7. **d3-IM5** decomposes into a chain structure, **d3-P2** (which is joined together with oxo and hydroxyl bridges), after H_2O leaves. From the free energy PES, it is clear that this channel is also energetically favorable. Two dehydration mechanisms of **d3-P2** were also investigated, as depicted in Fig. 8. However, these dehydration pathways are energetically unfavorable.

There is another dehydration channel leading to **d3-P2**. Likewise, via **d3-TS3**, the hydrogen atom on the bridging hydroxyl group of **d3-IM3** transfers to the OH group on the pentacoordinate Al atom (Fig. 7). The barrier and total barrier energies of this process are 118.1 and 51.7 kJ/mol^{-1}, respectively. The free energy barrier is comparable with the barriers associated with the path via **d3-TS2**.

Subsequently, we probed the condensation mechanism of **d3-IM3**, which leads to a cage-like structure, and the optimized parameters and PES profile for this are depicted in Fig. 9. **d3-IM3** can also be dehydrated to **d3-IM7** via **d3-TS4** with a free energy barrier of 101.2 kJ/mol^{-1}. After H_2O leaves **d3-IM7** to form **d3-P3**+H_2O, the Al–O–Al bond of

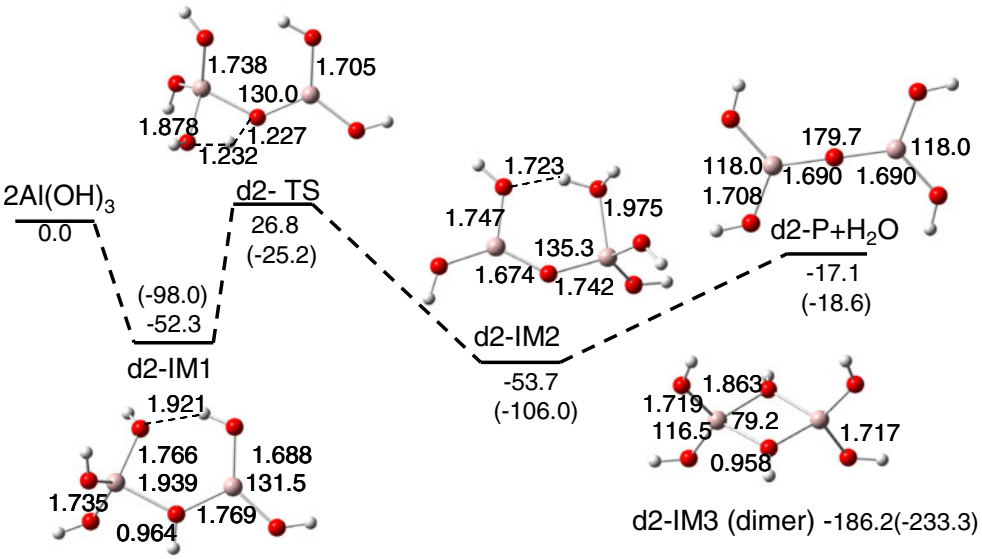

Fig. 5 Optimized structural parameters and the dehydration mechanism of **d2-IM1**

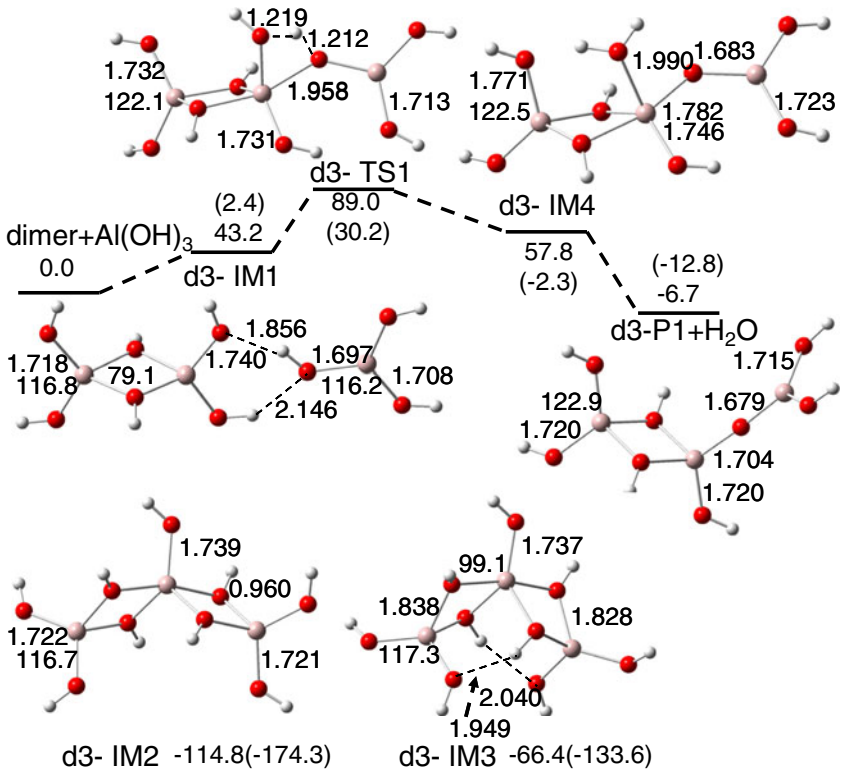

Fig. 6 Trimers of **d2-IM3**+Al$(OH)_3$ and the trimerization mechanism of **d3-IM1**

the tricoordinate Al atom is nearly linear. The relative energy of **d3-P3**+H_2O is high (63.6 kJ/mol^{-1}). However, one hydroxyl oxygen atom on the four-membered Al–O ring in **d3-P3** can complex to the tricoordinate Al atom via **d3-TS5** (with a low barrier of 25.1 kJ/mol^{-1}), generating **d3-P4**. Compared with **d3-IM3**, the relative free energy of **d3-P4** is 19.5 kJ/mol^{-1}. Since the complexation of the dimer and Al$(OH)_3$ releases a large amount of free energy, the cage-like channel will be energetically viable, but the chainlike geometries predominate in the oligomers before the aging of Al$(OH)_3$ aquasols. Therefore, under neutral conditions, the Al$(OH)_3$ precursor may first form tetracoordinate oligomers connected together by four-membered Al–O rings; these then develop into three-dimensional structures.

Conclusions

The mechanisms of Al$(OH)_3$ oligomerization in neutral and alkaline solutions were investigated by full optimization and single-point energy calculations with the CPCM solvation model at the B3LYP/6-311++G** basis set level. First of all, we examined the coordination modes and forms of Al$(OH)_3$ present, and found that the free energy reduction decreases significantly as the number of water molecules increases, so the Al atoms are tetracoordinate and pentacoordinate. In alkaline solution, the complexation of OH^- and Al$(OH)_3$ to form $[Al(OH)_4]^-$ decreases the free energy markedly (by 144.6 kJ/mol^{-1}). Moreover, the hydrogen-transfer barrier for $[Al(OH)_4]^-$ is large. Tetracoordinate aluminum compounds

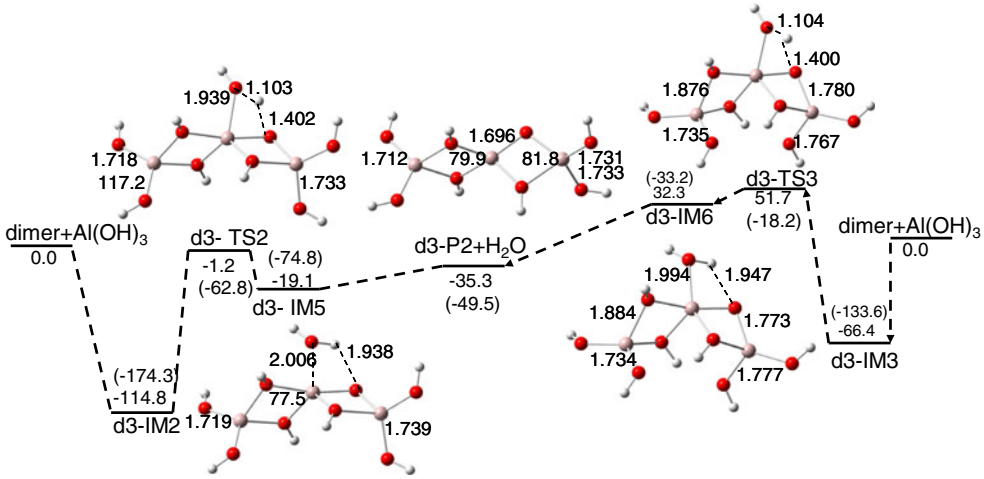

Fig. 7 S_N2 oligomerization mechanism of **d3-IM2**/**d3-IM3** +Al$(OH)_3$

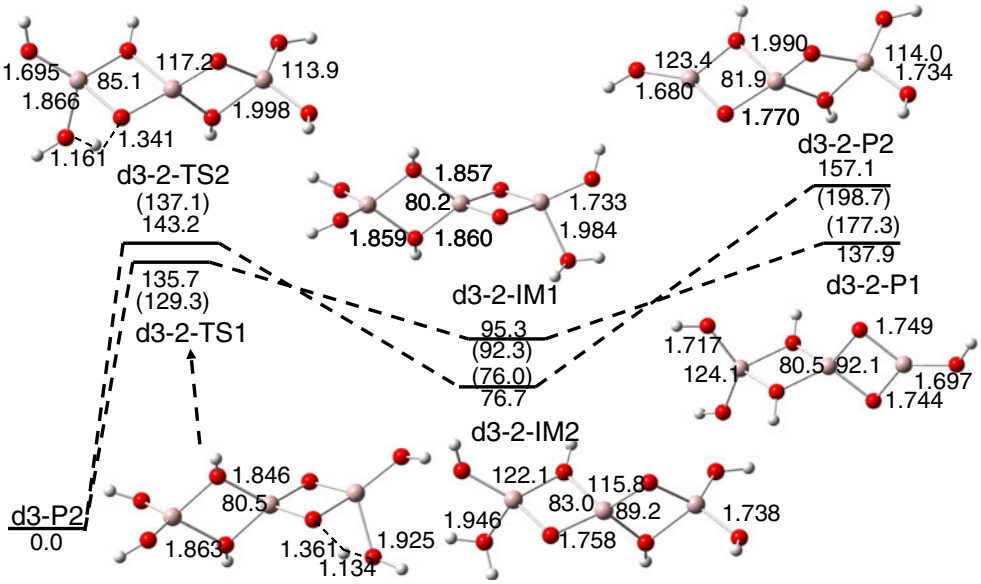

Fig. 8 Dehydration mechanisms of **d3-P2**

are therefore much more stable than tricoordinate ones, and the monomer does not exist as $[AlO(OH)_2]^-$.

The dimerization of $Al(OH)_3$ in alkaline solution was also investigated, and our computational results showed that $Al(OH)_3$ tends to condense into more soluble polyhydroxy compounds. The neutral dimerization of $Al(OH)_3$ and the transfer of the hydrogen of the bridging hydroxyl are energetically favorable, but the most stable geometry is a four-membered Al–O ring structure linked by two bridging hydroxyls, which decreases the free energy by −186.2 kJ/mol^{-1}.

The trimerization of the most stable dimer and $Al(OH)_3$ in neutral solution is very intricate. Here, the dehydration processes of three trimers were investigated. The theoretical model showed that the first step—the formation of four-membered Al–O rings—occurs easily, but the processes leading to cage-like structures involve higher barriers; dehydration of the second bridging hydroxyl hydrogen is also energetically unfavorable. In a word, $Al(OH)_3$ tends to spontaneously form tetracoordinate oligomers, which then develop into three-dimensional cage-like structures connected together by four-membered Al–O rings.

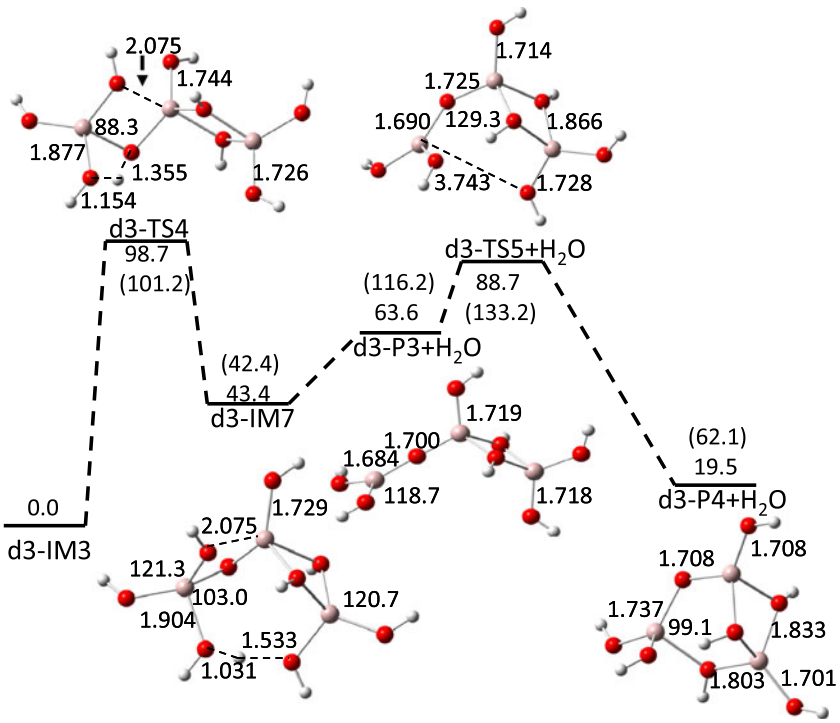

Fig. 9 Reaction mechanism for the conversion of **d2-IM3** into a cage-like structure

Acknowledgments This work was supported financially by the Natural Science Foundation of China (nos. 21173129 and 11174215) and the Natural Science Foundation of Shandong Province, China (no. ZR2012BL10).

References

1. Maloney R, Sakamoto J (2011) J Non-Cryst Solids 357:2059–2062
2. Wei G, Liu Y, Zhang X, Yu F, Du X (2011) Int J Heat Mass Transfer 54:2355–2366
3. Poco JF, Satcher JH Jr, Hrubesh LW (2001) J Non-Cryst Solids 285:57–63
4. Kistler SS (1931) Nature 127:741–741
5. Sarawade PB, Kim JK, Hilonga A, Quang DV, Jeon SJ, Kim HT (2011) J Non-Cryst Solids 357:2156–2162
6. Elanany M, Selvam P, Yokosuka T, Takami S, Kubo M, Imamura A, Miyamoto A (2003) J Phys Chem B 107:1518–1524
7. Zerda TW, Hoang G (1989) J Non-Crystal Solids 109:9–17
8. Scherer GW (1986) J Non-Cryst Solids 87:199–225
9. Shi F, Liu JX, Song K, Wang ZY (2010) J Non-Cryst Solids 356:2241–2246
10. Cheng X, Liu Y, Chen D (2011) J Phys Chem A 115:4719–4728
11. Pierre AC, Pajonk GM (2002) Chem Rev 102:4243–4265
12. König R, Scholz G, Veiczi M, Jäger C, Troyanov SI, Kemnitz E (2011) Dalton Trans 40:8701–8710
13. Kim J, Im H, Kim JM, Kim J (2012) J Mater Sci 47:1418–1426
14. Shi Z, Fu R, Agathopoulos S, Gu X, Zhao W (2012) Mater Design 34:820–824
15. Jiang L, Cui YZ, Shi YJ, Ding YD, Yuan FL (2011) Trans Nonferrous Met Soc China 21:2181–2185
16. Gu YB, Di Q, Lin MH, Tan K (2012) Comput Theor Chem 981:86–89
17. Williams GR, Moorhouse SJ, Prior TJ, Fogg AM, Rees NH, O'Hare D (2011) Dalton Trans 40:6012–6022
18. Li Y, Zhang Y, Chen F, Yang C, Zhang Y (2011) Cryst Growth Des 11:1208–1214
19. Swaddle TW, Rosenqvist J, Yu P, Bylaska E, Phillips BL, Casey WH (2005) Science 308:1450–1453
20. Saukkoriipi J, Laasonen K (2010) J Chem Theory Comput 6:993–1007
21. Saukkoriipi J, Laasonen K (2008) J Phys Chem A 112:10873–10880
22. Sarpola AT, Saukkoriipi JJ, Hietapelto VK, Jalonen JE, Jokela JT, Joensuu PH, Laasonen KE, Rämö JH (2007) Phys Chem Chem Phys 9:377–388
23. Saukkoriipi J, Sillanpää A, Laasonen K (2005) Phys Chem Chem Phys 7:3785–3792
24. Frisch MJ, Trucks GW, Schlegel HB, Scuseria GE, Robb MA, Cheeseman JR, Zakrzewski VG, Montgomery JA, Stratmann RE, Burant JC, Dapprich S, Millam JM, Daniels AD, Kudin KN, Strain MC, Farkas O, Tomasi J, Barone V, Cossi M, Cammi R, Mennucci B, Pomelli C, Adamo C, Clifford S, Ochterski J, Petersson GA, Ayala PY, Cui Q, Morokuma K, Malick DK, Rabuck AD, Raghavachari K, Foresman JB, Cioslowski J, Oritz JV, Stefanov B, Liu G, Liashenko A, Piskorz P, Komaromi I, Gomperts R, Martin RL, Fox DJ, Keith T, Al-Laham MA, Peng CY, Nanayakkara A, Gonzalez C, Challacombe M, Gill PMW, Johnson BG, Chen W, Wong MW, Andres JL, Head-Gordon M, Replogle ES, Pople JA (2004) Gaussian 03, revision D.01. Gaussian Inc., Wallingford
25. Wang HQ, Li HF, Wang JX, Kuang XY (2012) J Mol Model 18:2993–3001
26. Ho J, Klamt A, Coote ML (2010) J Phys Chem A 114:13442–13444
27. Archibong EF, Seeburrun N, Ramasami P (2009) Chem Phys Lett 481:169–172
28. Solans-Monfort X, Branchadell V, Sodupe M (2004) J Chem Phys 121:6034–6041
29. Swihart MT, Catoire L (2000) Combust Flame 121:210–222
30. Feyel S, Döbler J, Höckendorf R, Beyer MK, Sauer J, Schwarz H (2008) Angew Chem Int Ed 47:1946–1950
31. Wang Z, Wu X, Zhao Y, Ma J, Ding X, He S (2010) Chem Phys Lett 489:25–29
32. Cheng X, Zhao Y, Li L, Li Z (2010) Chin J Struct Chem 29:833–838
33. Wang Z, Wu X, Zhao Y, Ma J, Ding X, He S (2011) Chem Eur J 17:3449–3457
34. Wang Z, Dietl N, Kretschmer R, Weiske T, Schlangen M, Schwarz H (2011) Angew Chem Int Ed 50:12351–12354
35. Wang Z, Dietl N, Kretschmer R, Ma J, Weiske T, Schlangen M, Schwarz H (2012) Angew Chem Int Ed 51:3703–3707
36. Dietl N, Schlangen M, Schwarz H (2012) Angew Chem Int Ed 51:5544–5555
37. Hou H, Wang B (2005) J Phys Chem A 109:451–460
38. Gonzalez C, Schlegel HB (1990) J Phys Chem 94:5523–5527
39. Gonzalez C, Schlegel HB (1989) J Chem Phys 90:2154–2159
40. Cossi M, Scalmani G, Rega N, Barone V (2003) J Comp Chem 24:669–681
41. Ho J, Coote ML (2010) Theor Chem Acc 125:3–21
42. Lee TB, McKee ML (2012) Inorg Chem 51:4205–4214
43. Maggio E, Martsinovich N, Troisi A (2012) J Phys Chem C 116:7638–7649
44. Feytens D, Chaume G, Chassaing G, Lavielle S, Brigaud T, Byun BJ, Kang YK, Miclet E (2012) J Phys Chem B 116:4069–4079
45. Abreu CMR, Mendonça PV, Serra AC, Coelho JFJ, Popov AV, Gryn'ova G, Coote ML, Guliashvili T (2012) Macromolecules 45:2200–2208
46. Wang SC, Beal PA, Tantillo DJ (2010) J Comput Chem 31:721–725
47. Zhao Y, Truhlar DG (2008) Theor Chem Acc 120:215–241
48. Hohenstein EG, Chill ST, Sherrill CD (2008) J Chem Theory Comput 4:1996–2000
49. Kowall T, Caravan P, Bourgeois H, Helm L, Rotzinger FP, Merbach AE (1998) J Am Chem Soc 120:6569–6577
50. Bogatko S, Geerlings P (2012) Phys Chem Chem Phys 14:8058–8066